Journal of Neurocytology **14**, 887–907 (1985)

Axo-glial relations in the retina–optic nerve junction of the adult rat: freeze-fracture observations on axon membrane structure

JOEL A. BLACK[1], STEPHEN G. WAXMAN[1] and CLAES HILDEBRAND[2]

[1]*Department of Neurology, Stanford University School of Medicine and Veterans Administration Medical Center, Palo Alto, CA 94304, USA*
[2]*Department of Anatomy, Karolinska Institutet, Stockholm, Sweden*

Received 3 June 1985; accepted 24 July 1985

Summary

The axolemmal ultrastructure of nerve fibres within the retina–optic nerve junction (ROJ) from adult rats was examined by freeze-fracture electron microscopy. In the juxtaocular (proximal) region of the ROJ, all fibres are unmyelinated. The axons generally have a membrane ultrastructure similar to that of retinal nerve fibre layer axons, with a high density of intramembranous particles (IMPs) on the P-fracture face and a low density of IMPs on the E-face. However, along some axons in this region of the ROJ, localized aggregations of E-face IMPs are observed. At levels of the ROJ closer to the optic nerve proper, the unmyelinated fibres enter a transition zone in which the axons acquire myelin sheaths. By the distal boundary of the transitional zone (optic nerve proper), virtually all fibres are myelinated. Within the transitional zone, conventional axo-glial associations and axolemmal ultrastructure is present at nodes of Ranvier. In addition, atypical axo-glial relationships and atypical nodal segments are observed in this region. At some nodes, an isolated oligodendroglial process traverses obliquely across the nodal membrane. Beneath the oligodendroglial process, the axolemma usually displays a paranodal-like ultrastructure. Finger-like oligodendroglial processes were also observed in association with non-nodal unmyelinated axon membrane. At these sites of association, the axon membrane tends to be indented and may have a paranodal-like morphology. Nodal axolemma may exhibit several atypical forms in the transition zone. At some nodes, the nodal axolemma has a low density of E-face particles. Also, nodes of extended linear length (~2 μm) exhibit a lower-than-normal density of P-face IMPs. At heminodes, the axolemma immediately adjacent to the terminal loops lacks the usual nodal characteristics of high IMP density and high percentage of large particles. The results show that aberrant axo-glial associations accompanied by unusual ultrastructural characteristics of the axolemma are present in the ROJ of normal adult rats.

Introduction

Axons of adult rat retinal ganglion cells are unmyelinated throughout their course in the

0300–4864/85 $03.00 + .12

retina and become myelinated when they leave the eyeball and form the optic nerve. The transition occurs in the ROJ, which is totally unmyelinated in its juxtaocular aspect (optic nerve head) and virtually 100% myelinated where it joins the optic nerve proper. The transition from unmyelinated to myelinated fibre may require structural specialization of the axon and/or myelinating cell in order to ensure secure impulse conduction (Revenko *et al.*, 1973; Waxman & Brill, 1978; Quick *et al.*, 1979). Since the ROJ includes a spectrum of axo-glial relations that varies substantially along the fibre axis from totally unmyelinated to fully myelinated fibres, examination of this spatially restricted region should provide insight into the interactions between axons and glial cells which underlie CNS myelination.

The freeze-fracture ultrastructure of retinal nerve fibre layer axons (unmyelinated) and optic nerve fibres (myelinated) has been previously described (Black *et al.*, 1982a, 1983; Oldfield & Bray, 1982). However, little attention has been focused on the transition between these two regions (Black *et al.*, 1982b). Recently, the ROJ in the adult rat was examined in a detailed thin section EM study (Hildebrand *et al.*, 1985). Within the transition zone of the ROJ, this study showed a morphology similar to that observed along dysmyelinated fibres, including atypical axo-glial association, unusually thin and short myelin sheaths, and intermittent myelination. The present freeze-fracture investigation examines the question of whether the unusual axo-glial interactions in the ROJ affect axonal membrane ultrastructure. The present results indicate that unusual axo-glial associations are accompanied by ultrastructural changes in the axolemma. Thus, non-conventional axon membrane morphologies, previously only observed in dysmyelinated mutant species, are also present within the ROJ of normal adult rats.

Materials and methods

Six adult Long Evans rats, weighing 300–400 g, were used. The animals were anaesthesized with chloral hydrate (30 mg per 100 g, intraperitoneally) and perfused through the heart, first with a phosphate-buffered saline solution at room temperature and then with a solution of either 5% glutaraldehyde and 0.1 M sucrose in a 300 mOsm phosphate buffer or 2% glutaraldehyde and 2% paraformaldehyde in 0.14 M Sorensen's phosphate buffer. The fixative was delivered at room temperature via an adjustable speed roller pump and the flow was monitored with a drip chamber in the delivery line. Following perfusion for at least 20 min, the eyeballs were removed together with 3–5 mm of the optic nerves. Specimens, composed of the optic disc region of the eyebulb and the juxtaocular segment of the optic nerve, were dissected out and placed into fresh fixative.

Tissue for semithin sections was fixed overnight at 4° C. The specimens were then washed in phosphate buffer, postfixed in 2% OsO_4 in phosphate buffer for 2 h at 4° C, dehydrated in graded alcohols and embedded in Epon–Araldite. Semithin sections (1 μm) were stained with toluidine blue.

Specimens for freeze-fracture examination were immersed in fixative for 2–3 h at 4° C following perfusion. The tissue was washed several times in phosphate buffer and then cryoprotected, first with 10% glycerol in buffer (2–3 h) and then with 30% glycerol in buffer (overnight) at 4° C. The specimens were oriented on gold–brass specimen supports and rapidly frozen in a slush of Freon

22. Freeze-fracturing was performed in a Balzers BAF 301 freeze-etch device, with the stage temperature maintained at −115° C and the vacuum below 2×10^{-6} Torr. Platinum (2 nm) was deposited at a 45° angle and stabilized with a layer of carbon. Replicas were cleaned, first in bleach and then in 50% dichromate acid, rinsed several times in double-distilled water and mounted on Formvar-coated mesh grids. Replicas were examined with a JEOL 100CX electron microscope.

Quantification of IMP density was performed as previously described (Black *et al.*, 1981). Particle counts were determined by marking all particles within a given area and then measuring the transcribed area with a planimeter. Particle diameters were taken to be equivalent to the width of the shadow immediately behind the IMP, measured normal to the direction of shadowing.

Results

The ROJ is the site of transition between the unmyelinated fibres of the retinal nerve fibre layer (NFL) and the myelinated axons of the optic nerve proper (Fig. 1). The general morphology of this region has been described in a recent thin section study (Hildebrand

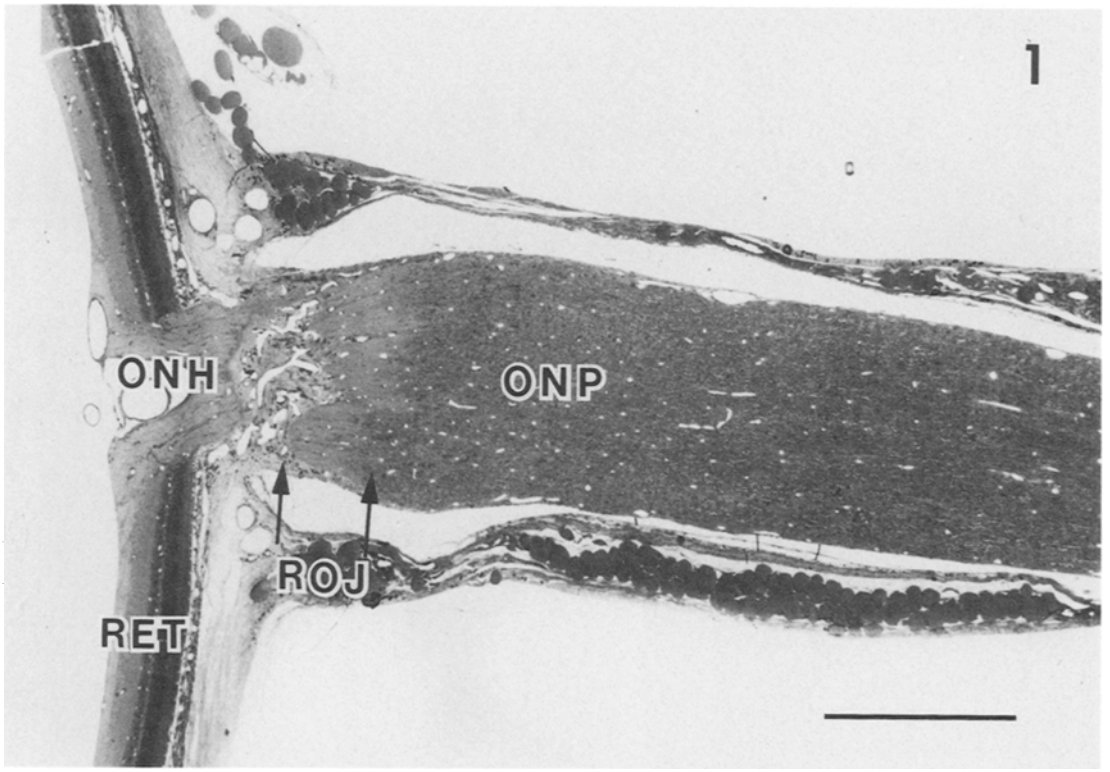

Fig. 1. Light micrograph of longitudinal semithin section through optic nerve proper (ONP), retina–optic nerve junction (ROJ), and retina (RET) of an adult Long Evans rat. Axons in the nerve fibre layer of the retina and in the optic nerve head (ONH) are unmyelinated. Within the ROJ (arrows), fibres become myelinated and in the ONP virtually all axons are myelinated. × 50. Scale bar: 500 μm.

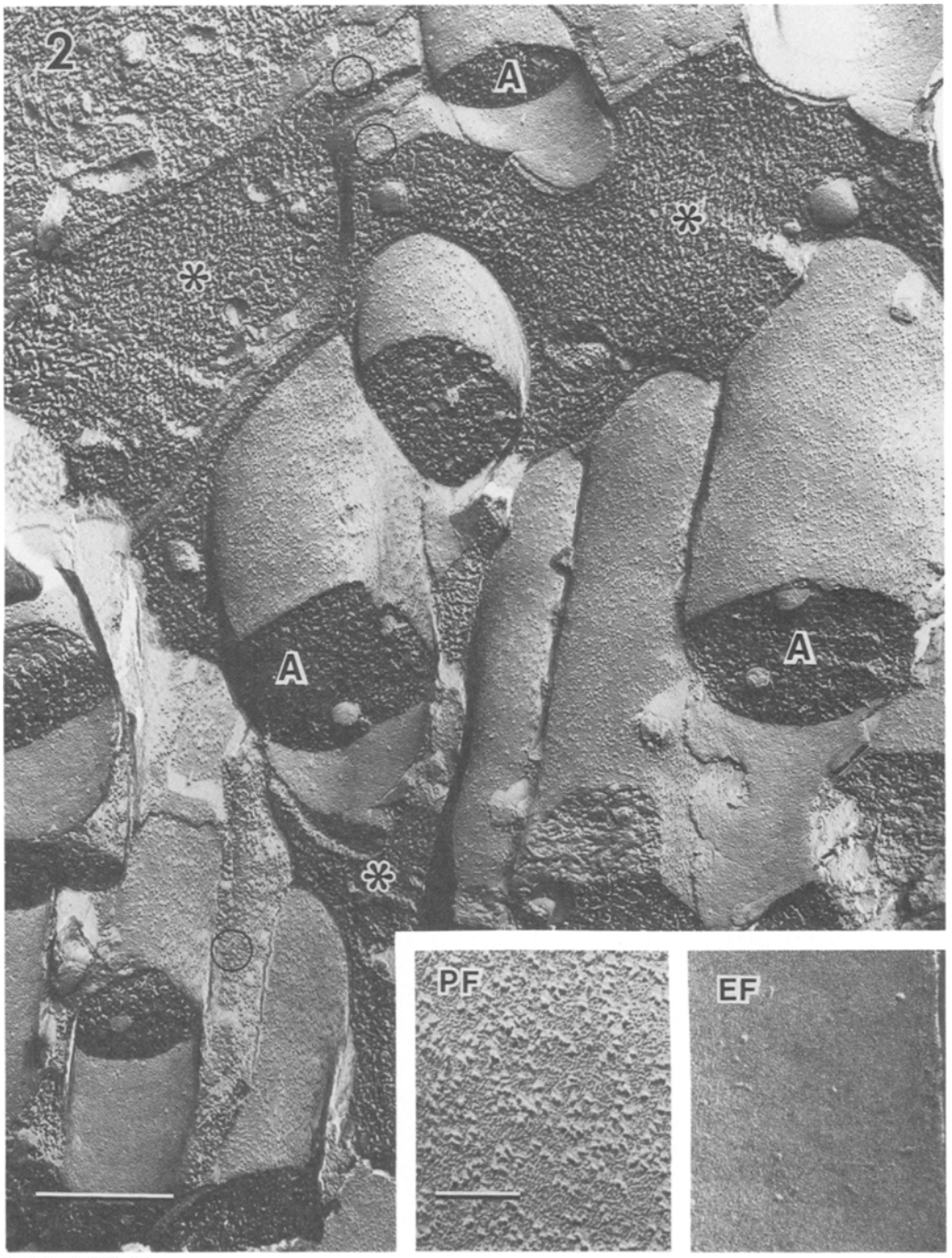

Fig. 2. Freeze-fracture electron micrograph of the juxta-ocular region of the ROJ from an adult Long Evans rat. All the fibres (A) are unmyelinated and are surrounded by astrocytic processes (asterisks). Note the orthogonal arrays of particles (encircled) on the P-faces of astrocytic membrane. × 40 000. Scale bar: 0.5 μm. Insets: the asymmetrical partitioning of particles on the fibres within this region is shown at higher magnification. The P-face (PF) is highly particulate, while few IMPs are present on the E-face (EF). × 125 000. Scale bar: 0.1 μm.

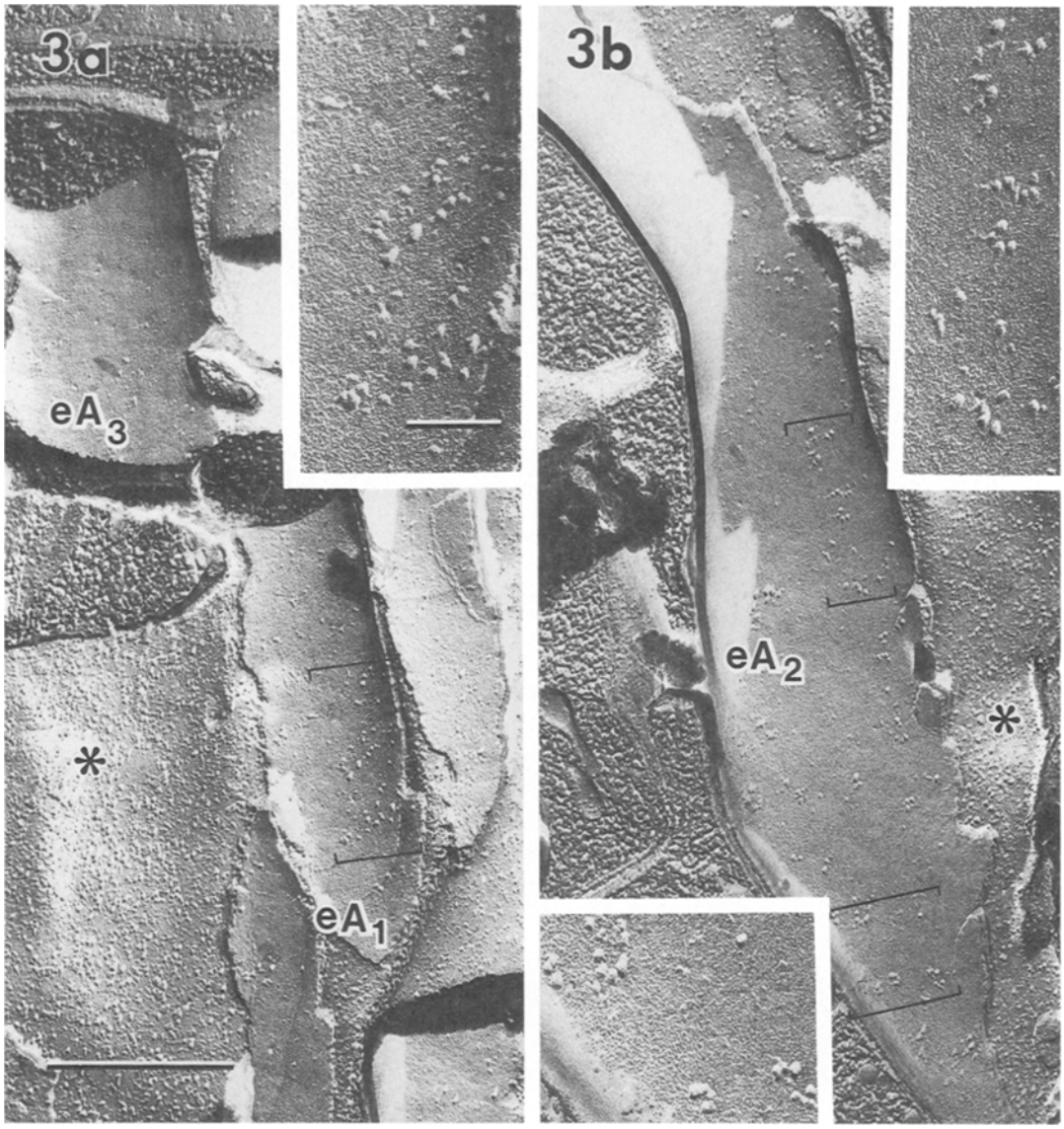

Fig. 3. (a) and (b) Freeze-fracture electron micrograph of juxta-ocular region of the ROJ. Some of the axons (eA_1, eA_2) in this region exhibit an increased density of E-face IMPs. An adjacent axon (eA_3) has a low density of particles. Astrocytic processes (asterisks) are prevalent in this region. × 50 000. Scale bar: 0.5 μm. Insets: the areas in brackets are shown at increased magnification. Note that many IMPs have a large diameter (>9.6 nm). × 125 000. Scale bar: 0.1 μm.

et al., 1985), and the freeze-fracture ultrastructure of nerve fibre layer axons and optic nerve proper fibres has also been previously described (Black *et al.*, 1982a, 1983).

In freeze-fracture replicas, fibres of the ROJ are easily distinguished from axons of the

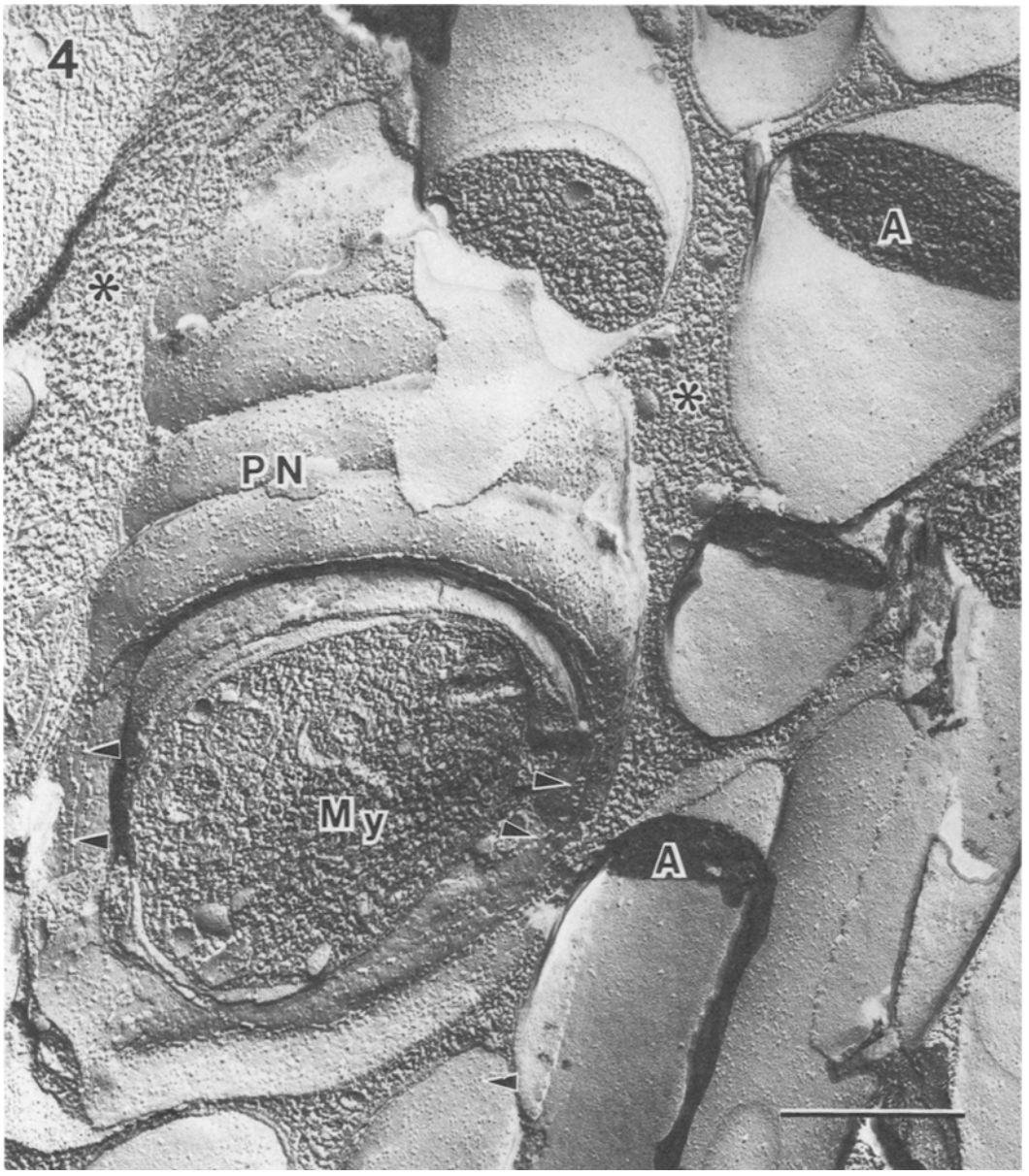

Fig. 4. Freeze-fracture electron micrograph of a myelinated fibre (My) amongst unmyelinated axons (A) in the transition zone of the ROJ. The fracture plane removes the covering myelin lamellae and exposes the P-faces of oligodendrocytic paranodal loops (PN) not in immediate apposition to axolemma. Tight junctions (arrowheads) are observed between adjacent paranodal loops. Note that all fibres are surrounded by astrocytic processes (asterisks). × 50 000. Scale bar: 0.5 μm.

NFL and the optic nerve. In the juxta-ocular region of the ROJ, the fibres are all unmyelinated and are surrounded by astroglial processes (Fig. 2). Axons in this region have a membrane morphology generally similar to that of fibres of the NFL, with a high density of IMPs on P-fracture faces and a low density of particles on E-faces (Fig. 2 insets). There are, however, regions where the axolemmal E-face has a locally increased density of particles. These areas can be relatively punctate or can extend for 1–2 μm along the length of the axon (Fig. 3a, b). While the E-face IMP density of these localized regions (~500 μm^{-2}) is significantly lower than that observed at nodes (~1300 μm^{-2}), the particle density of these areas is substantially greater than that generally present on unmyelinated E-faces of fibres in the NFL (~225 μm^{-2}). A high percentage of the IMPs in these regions of increased density are large particles (>10 nm in diameter), and many of these large IMPs tend to be aggregated into groups of between four and eight (Fig. 3a, b insets). Since the axons in this region are totally embedded in astrocytic processes, it is not possible to determine specific glial-axonal relationships at the regions of increased IMP density. Moreover, oligodendrocytic processes are not present in this portion of the ROJ, and specialization of the axon membrane, as seen at paranodal regions, is not observed in areas of increased E-face IMP density.

At ROJ levels closer to the optic nerve proper, occasional myelinated axons are encountered between the more numerous unmyelinated axons (Fig. 4). This is the beginning of the transition zone of the ROJ. In this portion of the zone, astrocytic processes continue to surround all fibres; unmyelinated as well as myelinated axons are ensheathed by the astrocytic processes. Myelinated fibres are of larger diameter than unmyelinated axons, being typically ~1 μm in diameter compared to ~0.5 μm for unmyelinated fibres. As the transition zone is traversed, the proportion of myelinated fibres increases. In addition, astrocytic processes gradually become less abundant and oligodendroglial processes become increasingly frequent. Within the transitional zone, fibre segments exhibiting typical nodal and paranodal ultrastructure, can be found (Fig. 5a, b), as observed in the optic nerve proper. At such sites, both fracture faces of nodal membrane are highly particulate (~1200–1300 μm^{-2}), with each face displaying a high percentage (~50%) of large particles (Fig. 5a, b insets). The fracture faces of paranodal axolemma show characteristic scalloped patterns, coinciding with the helically wound terminal oligodendroglial loops (Fig. 5a, b). Paranodal P-faces of the axolemma appear as a series of flattened indentations separated by narrow ridges, while on E-faces shallow, slightly convex surfaces are separated by narrow grooves.

In addition to the usual spatial arrangement and ultrastructure of axonal and glial components at nodes of Ranvier, distinctly irregular patterns of axo-glial interactions and axolemmal ultrastructure are also observed in the transition zone of the ROJ. In several of the nodes of Ranvier encountered, the node is bounded by conventional paranodal loops, but an additional glial process traverses obliquely across the nodal membrane (Figs 6–8). It was not always possible to identify unequivocally the glial cell type of this finger-like process, but when this was possible the parent cell was always an oligodendrocyte. In all cases encountered, the nodal membrane is indented where it is

apposed by an errant glial process. The indented strip of nodal membrane lacks nodal characteristics (i.e. high density of IMPs and high percentage of large particles). Instead, the axolemma usually assumes an appearance typical for paranodal axolemma (Figs 6–8). On the P-face, this paranodal-like specialization is manifest as rows of particles oriented parallel to the long axis of the overlying glial process (Fig. 7). The spacing between the faintly-observed rows of particles is ~30 nm (Fig. 7 inset). This is similar to the periodicity of the diagonal rows of IMPs within conventional paranodal P-face axolemma. The E-face of the indented strip of nodal axolemma also has paranodal-like appearance (Fig. 8). The axon membrane exhibits linear striations oriented parallel to the apposing glial process (Fig. 8 inset). Due to the plane of fracture, it is not possible to determine if the indenting glial processes in these and similar examples originates from one of the adjacent myelin termination regions. In addition, it is not clear to what extent such processes encircle the node.

In the transition zone, finger-like processes of oligodendrocytes were also observed in association with unmyelinated axonal segments. In Fig. 9a, an oligodendroglial process passes beneath one unmyelinated axon and then over an adjacent unmyelinated fibre. Both axons show paranodal-like membrane specializations at the site of axo-glial association. In the region where the oligodendrocytic process runs beneath the axon, the axolemma is distinctly invaginated. The E-fracture face of the indented strip of axon membrane has an ultrastructure similar to that observed on paranodal E-face axolemma in myelinated axon segments (cf. Fig. 5b), with several slightly oblique rows of IMPs (Fig. 9c). Interestingly, this linear pattern maintains its slightly oblique orientation relative to the glial process although the process changes direction. Emerging from beneath the fibre, the oligodendrocytic process is briefly visible before it passes over an adjacent unmyelinated axon. This fibre segment is clearly indented by the glial process (Fig. 9a), and the indented axolemma displays paranodal-like membrane specialization on the exposed P-face. Rows of IMPs with a periodicity of ~30 nm are observed parallel to the process (Fig. 9b). This spacing of adjacent rows is similar to that of the P-faces of paranodal axolemma of myelinated fibres (cf. Fig. 5a). In the example shown here, it is clear that the glial process does not encircle either apposed axon. Nevertheless, each fibre is indented at the site of axo-glial association.

The vast majority of nodes of Ranvier observed in the transition zone of the ROJ have highly particulate E- and P-fracture faces (cf. Fig. 5a, b). However, several cases of E-face

Fig. 5. Freeze-fracture electron micrographs from the ROJ showing P-face (a) and E-face (b) of nodal (N) and paranodal (PN) axon membrane at a conventional node of Ranvier. On both fracture faces the nodal membrane is highly particulate. The paranodal axolemma has a scalloped appearance corresponding with the terminal oligodendroglial loops (arrowheads). The P-face of the paranodal axolemma exhibits rows of IMPs within the indented areas, while a faint rope-like appearance is evident on the E-face. × 50 000. Scale bar: 0.5 μm. Insets: nodal P- and E-faces are shown at increased magnification. Note the high percentage of large particles (arrowheads). × 125 000. Scale bar: 0.1 μm.

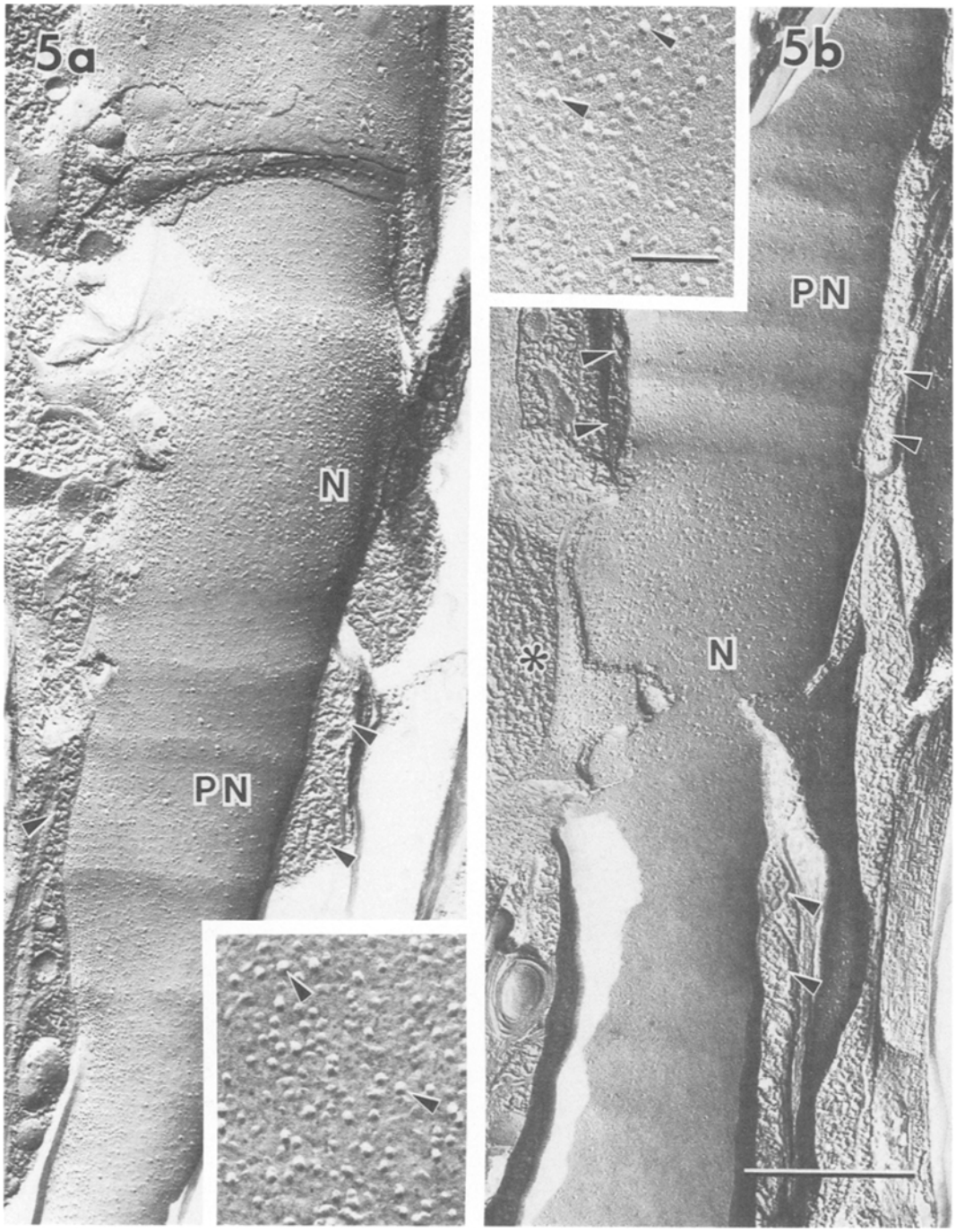
5a
N
PN
5b
PN
N

nodal membrane lacking a high density of IMPs were observed at nodes of Ranvier. In the example shown in Fig. 10, the fracture plane exposes P-face paranodal axolemma on either side of the node. The fracture plane then cross-fractures through the axoplasm to reveal the E-face of the node enclosed by the paranodal loops. The paranodal axon membrane has a conventional ultrastructure. The axon membrane at the node, however, has an extremely low density of E-face particles ($\sim 130\,\mu m^{-2}$), being similar to that of internodal axon membrane. Despite the low density of IMPs, a high percentage of these IMPs are of a large size (>9.6 nm in diameter) (Fig. 10 inset). Astrocytic processes are in immediate proximity to the node and appear to encircle it (Fig. 10).

For most nodes of Ranvier observed in the transition zone of the ROJ, the length of the nodal gap is <1.0 μm (mean ± S.D. = 0.83 ± 0.17 μm; n = 23). However, some nodes with gap lengths of up to ~2.0 μm were encountered. Nodes with extended lengths appear to be less particulate than nodes with conventional lengths, having a P-face IMP density of $\sim 800\,\mu m^{-2}$ (Fig. 11). In addition, the percentage of large particles (>9.6 nm in diameter) in such expanded 'nodal' regions (~20%) is substantially less than in more typical nodes of Ranvier (~50%) (Fig. 11 inset).

Fibre segments with heminodal morphology (i.e. only a single set of myelin sheath terminations beyond which the fibre continues unmyelinated) were occasionally encountered. From the final terminal loop of the heminodal myelin sheath termination, the nonmyelinated segment was observed to extend up to ~6 μm before the fracture plane left the fibre. Immediately adjacent to the myelin sheath termination in heminodal regions, the axon membrane usually lacks typical nodal membrane specialization. This is most easily observed on the E-face (Figs 12a, 13) where the density of IMPs adjacent to the terminal oligodendrocytic loops was much lower than at conventional nodes. Small aggregations of IMPs sometimes occurred in these heminodal regions, with many of the particles being large-sized (Figs 12c, 13). Progressing along the axon away from the terminal loops, the density of E-face IMPs rapidly approaches the low IMP density typical for conventional unmyelinated axolemma (Fig. 12b).

Fig. 6. Freeze-fracture electron micrograph of a node of Ranvier within the transition zone of the ROJ. To the left of the node (N), terminal oligodendrocytic loops (OL) are observed, whereas to the right of the node, paranodal axolemma (PN) is shown. The P-face of the node (N) is indented by an aberrant process traversing across it (between arrows). Note that beneath the glial process the axolemma lacks nodal membrane characteristics. × 50 000. Scale bar: 0.5 μm.

Fig. 7. Freeze-fracture electron micrograph of a nodal region within the transition zone of the ROJ. The terminal oligodendrocytic loop (OL) is exposed to the right of the node. The P-face of the nodal axolemma (N) is obliquely traversed by a glial process (between arrows) which indents the nodal axolemma. The strip of axolemma beneath the glial process exhibits a paranodal-like membrane specialization. × 50 000. Scale bar: 0.5 μm. Inset: the region beneath the glial process is shown at increased magnification. Rows of particles (arrowheads) are observed within the axolemma. Note the high concentration of large particles present in the adjacent nodal membrane. × 125 000. Scale bar: 0.1 μm.

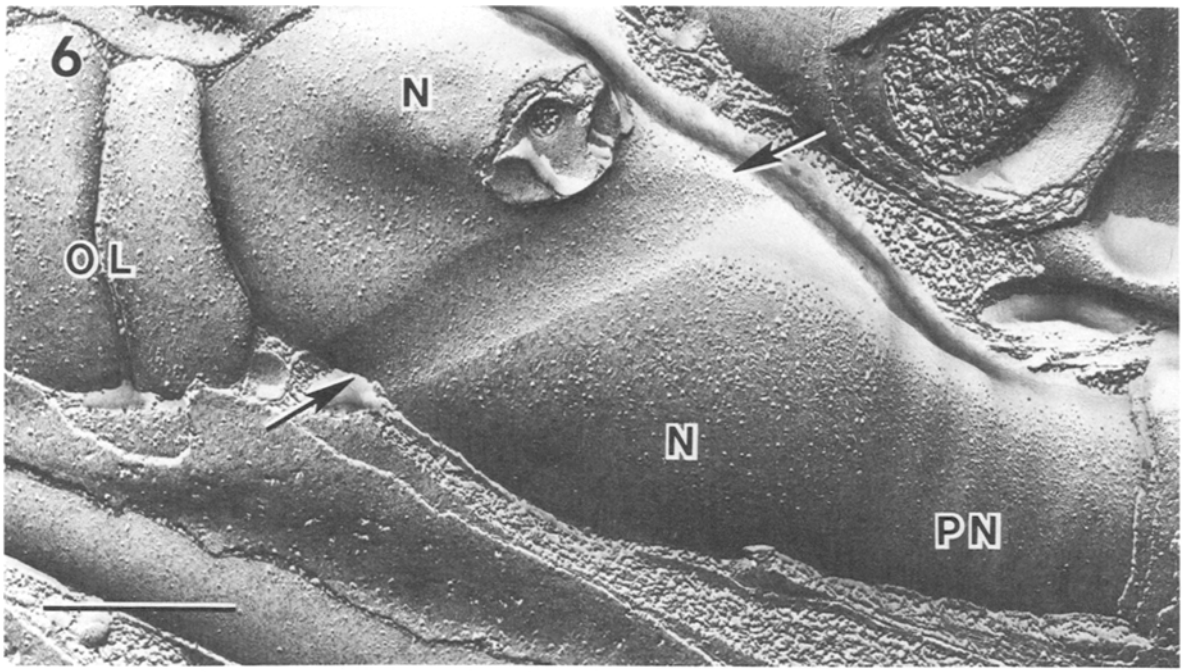
6
N
OL
N
PN

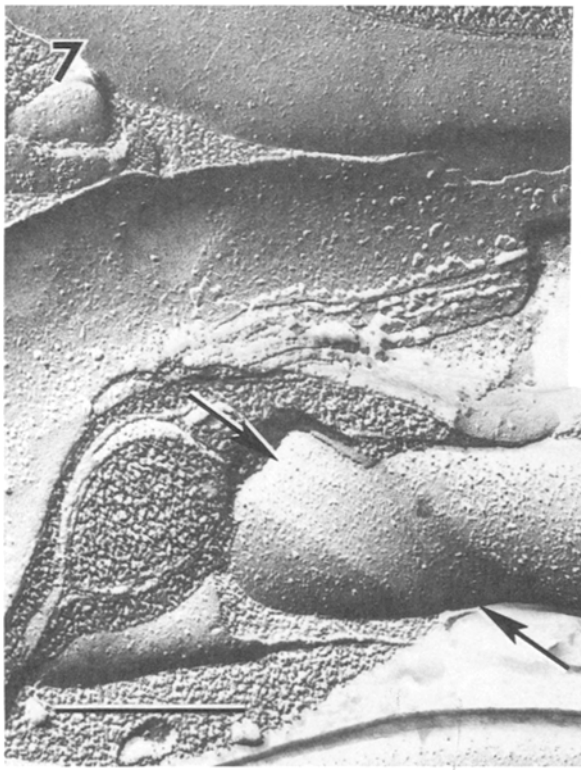
7
N
OL

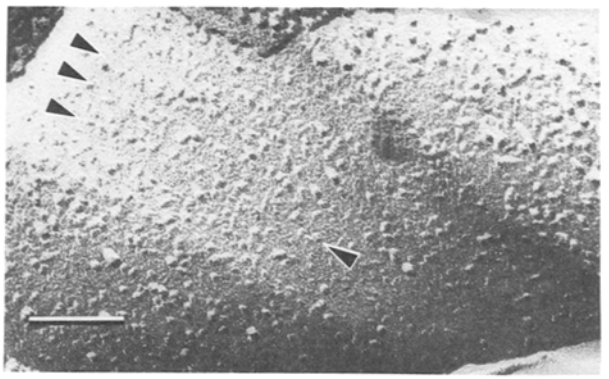

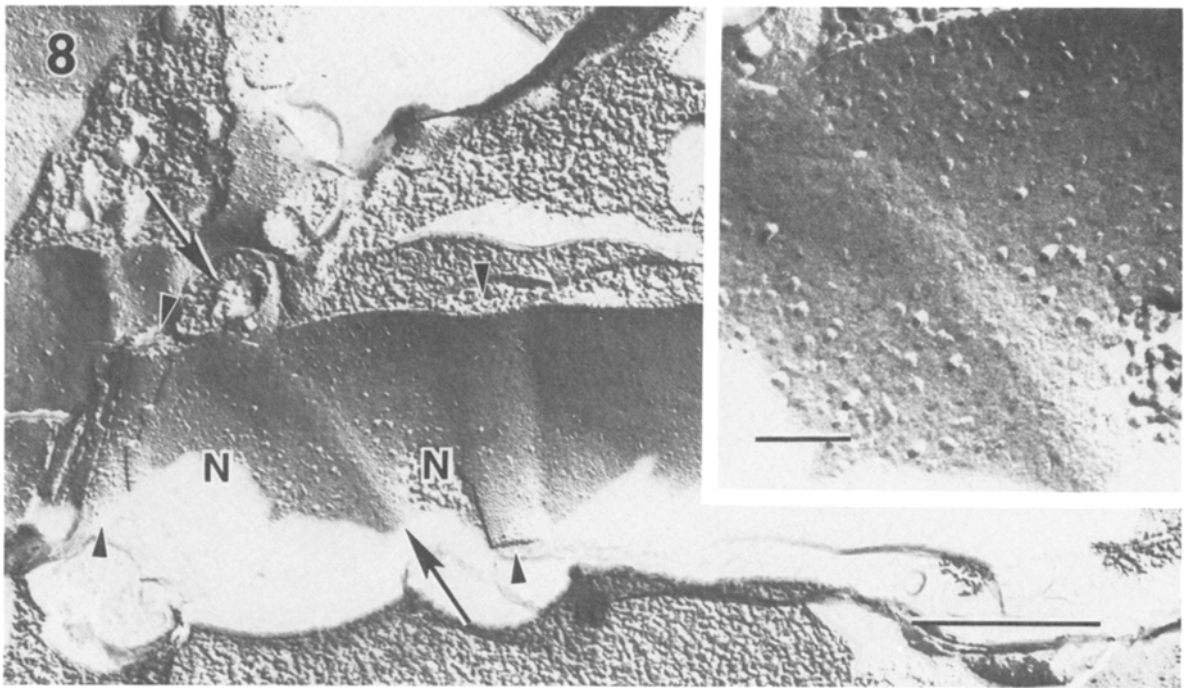

Fig. 8. Freeze-fracture electron micrograph of the E-face of nodal and paranodal axolemma in the transition zone of the ROJ. The nodal axon (N) is delimited by terminal paranodal loops (arrowheads) and is traversed obliquely by a glial process (between arrows). Beneath the aberrant glial process the axolemma is indented and exhibits a paranodal-like specialization. × 50 000. Scale bar: 0.5 μm. Inset: region of axon membrane beneath aberrant process is shown at increased magnification. The membrane has a faintly striated appearance. Note the high density of IMPs in the adjacent nodal membrane and the scarcity of large particles in the region beneath the glial process. × 125 000. Scale bar: 0.1 μm.

Fig. 9. Freeze-fracture electron micrograph of an aberrant oligodendroglial process within the transition zone of ROJ. (a) A finger-like oligodendrocytic process passes beneath an axon (eA_1) and then over an adjacent axon (pA_2). Both axons are indented by the glial process and both fibres exhibit paranodal-like membrane specialization at the sites of glial apposition. × 50 000. Scale bar: 0.5 μm. (b), (c) Areas in brackets are shown at increased magnification. The aberrant process (asterisk) exhibits characteristic oligodendrocytic P-face IMPs (i.e. large and tall IMPs, small and short particles and no orthogonal arrays of IMPs). On the axolemmal P-face (pA_2 in Fig. 9a), slightly disorganized rows of IMPs are observed oriented parallel to the overlying process. The E-face (eA_1 in Fig. 9a) of axolemma beneath the oligodendrocytic process exhibits rows of IMPs in a rope-like pattern. The rows maintain a slightly oblique orientation in relation to the glial process even when it changes direction. × 125 000. Scale bar: 0.1 μm.

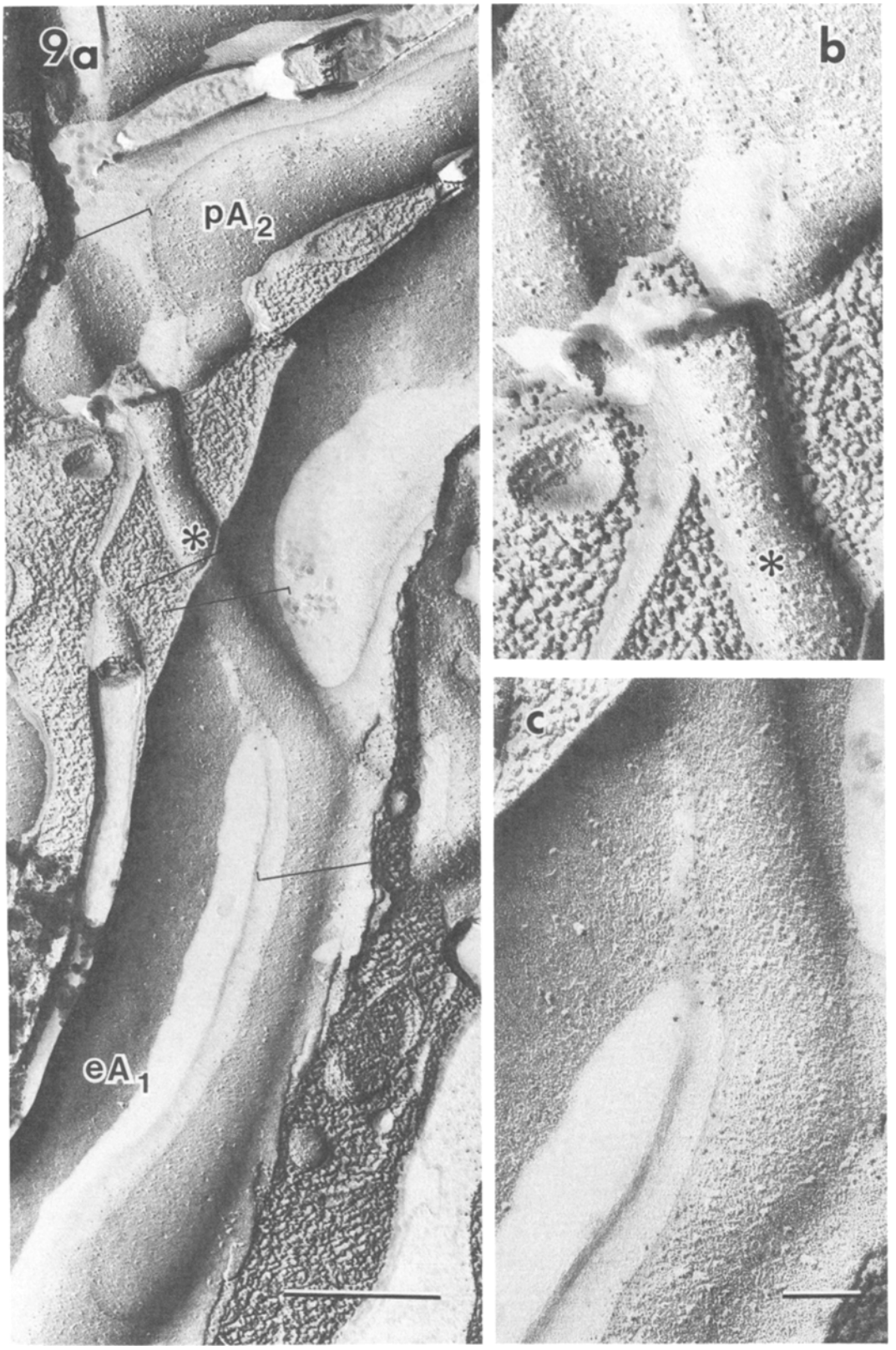
9a
pA2
*
eA1
b
*
c

Discussion

The results presented here demonstrate that the transition zone of the ROJ is a complex region, exhibiting aberrant axo-glial associations, irregular membrane specializations and a range of nodal morphologies. At juxta-ocular levels of the ROJ, all fibres are unmyelinated and surrounded by astroglial processes. Oligodendrocytes are not observed in this region. As the ROJ is traversed distally, the proportion of myelinated fibres increases gradually over hundreds of micrometres (Hildebrand *et al.*, 1985). Moreover, as seen along any single axon, the transition between unmyelinated and myelinated regions involves a transitional domain of atypical axo-glial associations. Within the transition zone, many of the fibres have a morphology similar to that of dysmyelinated axons (Hildebrand *et al.*, 1985). Finally, at levels where ROJ merges into the optic nerve proper, virtually all axons are myelinated and exhibit a conventional ultrastructure.

Unmyelinated fibres in the juxta-ocular aspect of the ROJ display spatial heterogeneity of the axolemma. In this respect, these unmyelinated ROJ fibres, like unmyelinated axons in the retinal nerve fibre layer (Hildebrand & Waxman, 1983; Black *et al.*, 1984), exhibit a different structure from most unmyelinated fibres (Black *et al.*, 1981). Both patchy (this study) and linearly-banded (Black *et al.*, 1982b) regions of increased E-face IMP density are evident within the membrane of these unmyelinated ROJ axon segments, being clearly discernible from the generally low density of particles in surrounding areas of the unmyelinated axolemma. This pattern of localized increased E-face IMP density is similar to that observed within specialized regions along axons of the retinal NFL (Black *et al.*, 1984), although the density of E-face particles in the node-like regions of the NFL axons is somewhat greater than for fibres of the juxta-ocular ROJ ($\sim 825\,\mu m^{-2}$ versus $\sim 500\,\mu m^{-2}$, respectively). In this context, it should be noted that NFL axons with axolemmal patches of increased E-face density exhibit specifically associated Müller cell processes (Hildebrand & Waxman, 1983; Black *et al.*,

Fig. 10. Freeze-fracture electron micrograph of nodal region in transition zone of the ROJ. The nodal axolemma (eN) is delimited on both sides by paranodal axolemma (PN) with typical P-face membrane specializations. The exposed E-face of the nodal membrane has a very low density of IMPs. Note that an astrocytic process (asterisk) is in close proximity to the node. × 32 500. Scale bar: 1.0 μm. Inset: the nodal axolemma is shown at increased magnification. Few particles are present within the E-face nodal membrane, though several large IMPs are observed. An orthogonal array of IMPs of the juxta-nodal astrocytic process is encircled. × 125 000. Scale bar: 0.1 μm.

Fig. 11. Freeze-fracture electron micrograph of nodal region with an unusually long nodal gap length in the transition zone of the ROJ. The nodal axolemma (pN) is delimited by paranodal regions; on the left side a terminal oligodendroglial loop is apparent (OL), and on the right side the axolemma is indented by the terminal glial loop (arrowheads). The P-face of the nodal membrane has only a moderate density of particles. Several astrocytic processes (asterisk) are located adjacent to the nodal region. × 50 000. Scale bar: 0.5 μm. Inset: increased magnification of the nodal axolemma. Many of the particles present are large. × 125 000. Scale bar: 0.1 μm.

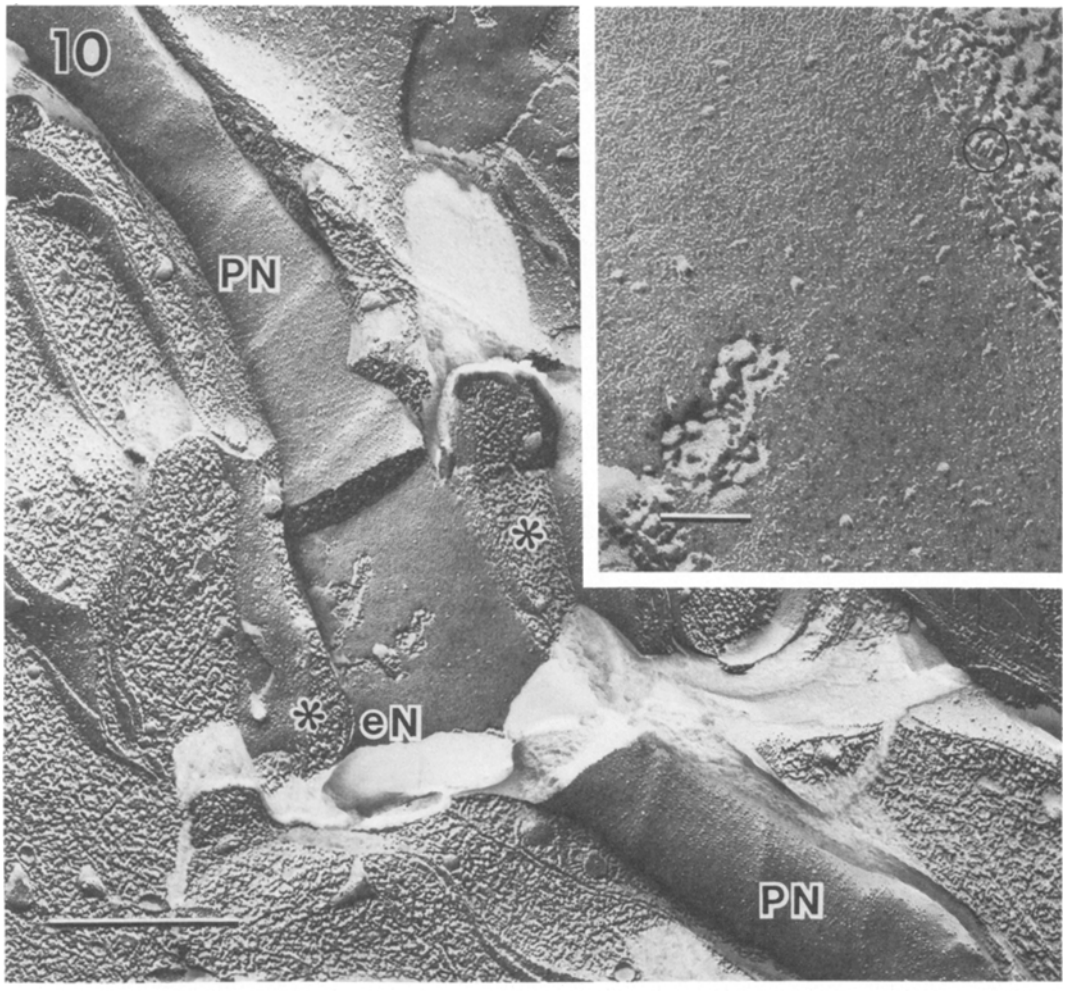
10
PN
eN
PN

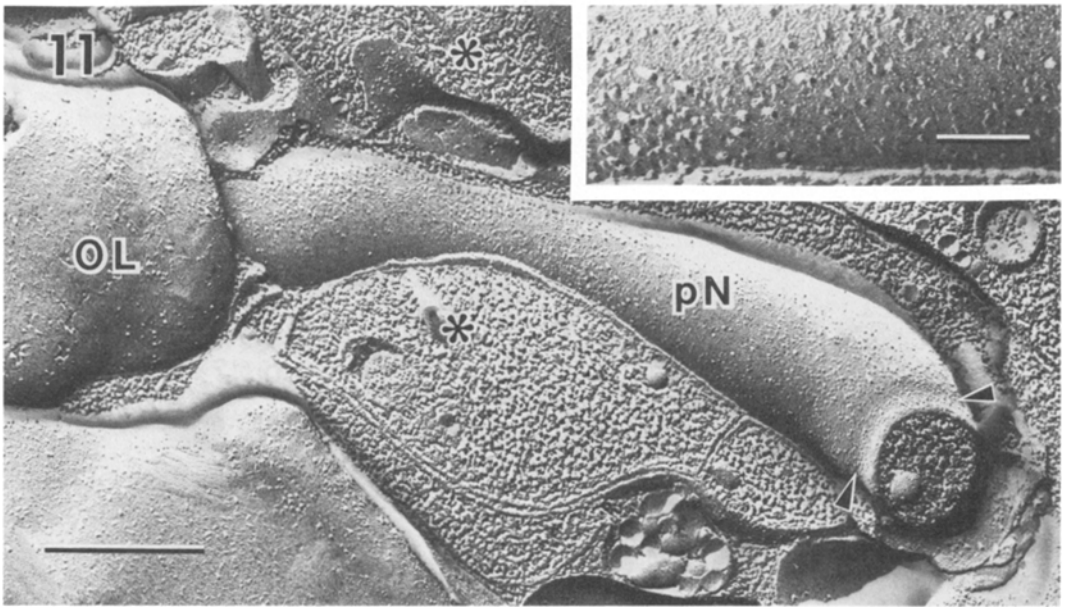
11
OL
pN

1984). In the juxta-ocular ROJ, however, a comparable distinct relationship between sites of increased E-face density in unmyelinated axolemma and glial processes has not been observed, possibly due to the presence of an encompassing matrix of astrocytic processes. Thus, the possibility of an inductive axo-glial interaction between glial processes and particle-rich axolemma within the unmyelinated membrane in the ROJ cannot be resolved at this time.

Nodes of Ranvier are characterized by a dense axolemmal undercoating (Elfvin, 1961; Peters, 1966) and a high E-face IMP density (Rosenbluth, 1976; Kristol *et al.*, 1978). In addition, nodes are thought to be sites of high densities of voltage-sensitive sodium channels (Conti *et al.*, 1976; Ritchie & Rogart, 1977; Waxman, 1977). In this regard, patches of electron-dense axolemmal undercoating have been described in unmyelinated fibres in the juxta-ocular part of the ROJ (Hildebrand *et al.*, 1985). These regions may correlate with the areas of high E-face IMP density described here. Such a correlation has been suggested in the NFL, where the similarity in ultrastructural relationships revealed by freeze-fracture (Black *et al.*, 1984) and thin section (Hildebrand & Waxman, 1983) make it likely that undercoated regions of axonal membrane contain a high density of E-face IMPs. Moreover, in such regions with a high density of IMPs, the percentage of large (>9.6 nm in diameter) E-face particles is high. It has been proposed that large IMPs might represent voltage-sensitive sodium channels (Rosenbluth, 1976; Kristol *et al.*, 1977). If this hypothesis is correct, it might be suggested that there is a close relationship between axolemmal undercoating and the occurrence of high concentrations of sodium channels. The previous observations in the ROJ of nodes and heminodes lacking axolemmal undercoating (Hildebrand *et al.*, 1985) and the present descriptions of axolemma with very low E-face particle densities in these regions are consistent with this view.

In the present study, examples of specific interactions between astrocytic processes and axolemma (as observed at CNS nodes of Ranvier; see e.g. Hildebrand 1971; Hildebrand & Waxman, 1984) were not apparent. However, relatively conventional

Fig. 12. Freeze-fracture electron micrograph of heminodal axon membrane within the transition zone of the ROJ. (a) In this low magnification view, an axon (eA) is indented by terminal paranodal loops (arrowheads) in the right part of the micrograph. To the left of this paranodal region the fibre remains unmyelinated. Areas in brackets are shown at increased magnification in (b) and (c) × 15 000. Scale bar: 2 μm. (b) In regions distant from the heminodal area, the density of particles on the E-face is low. (c) Adjacent to the final paranodal loop (arrowheads), the heminodal membrane (eN) exhibits some areas with particle aggregations, but it generally has a moderately low density of IMPs. × 125 000. Scale bar: 0.1 μm.

Fig. 13. Freeze-fracture electron micrograph of heminodal axolemma within the transition zone of ROJ. In this view at high magnification, a portion of the glial membrane of the terminal paranodal loop (PN) opposite the axolemma is exposed (i.e. 'beneath' the fracture face PN is extracellular space). The E-face (eN) of the axolemma adjacent to the final paranodal loop exhibits a density of particles much lower than normally observed at nodes. Note that several of the IMPs are of a large size (arrowheads). × 125 000. Scale bar: 0.2 μm.


12a
eA

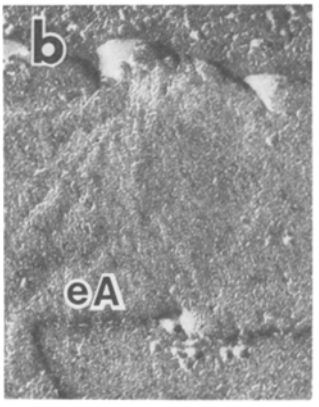
b
eA

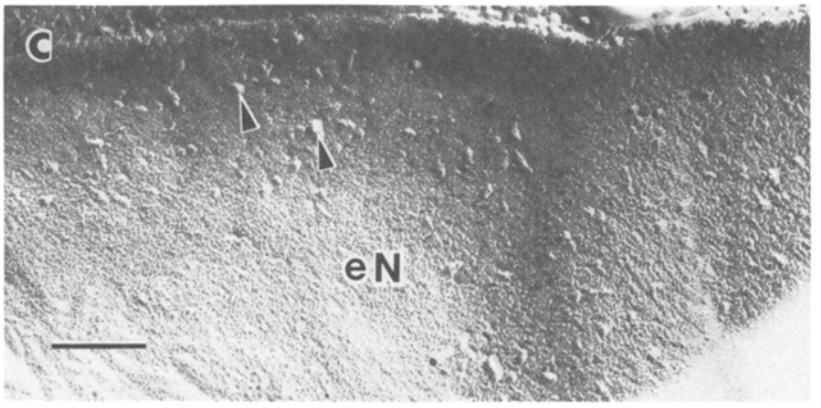
c
eN

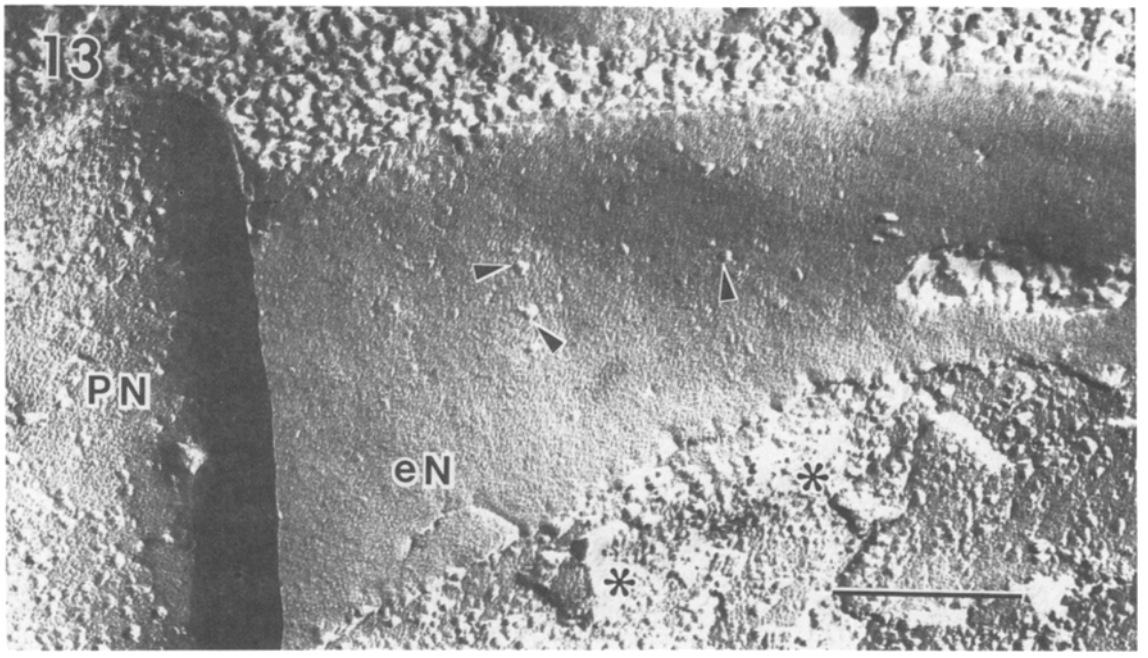
13
PN
eN

paranodal junctions and several types of atypical association between axon membrane and oligodendrocytic processes were observed. Apparently, intimate association between an oligodendroglial process and an axon induces change in the underlying axolemmal ultrastructure. In both nodal and non-nodal unmyelinated regions, the axon membrane beneath the glial process is indented and usually assumes a paranodal-like membrane ultrastructure. Similar membrane specializations have been reported at sites of aberrant glial–axon association in both the PNS and CNS of mutant mice (Rosenbluth, 1979, 1981a, b) and in the CNS of the canine 'shaking pup' mutant (Bray *et al.*, 1983). In dystrophic mouse spinal roots, the region of association between Schwann cell processes and amyelinated fibres is characterized by a paracrystalline-like appearance, which is reminiscent of paranodal membrane specialization (Rosenbluth, 1979). Among several other myelin-forming deficiencies, the mouse mutant Shiverer displays bizarre paranodal junctions between oligodendroglial processes and axolemma (Rosenbluth, 1981a). At each of these sites of aberrant association, the axon membrane assumes a paranodal-type ultrastructure even when the apposing glial process is oriented parallel to the axon. The above observations suggest an inductive influence of closely apposed oligodendrocytic processes on axolemmal ultrastructure. As shown in the present study, similar atypical axo-glial relations may occur at sites such as the ROJ. It has been suggested that abnormalities in myelination and axo-glial association of the mutants described above are the result of disorder during the development of axo-glial interactions (Bray *et al.*, 1981; Aguayo & Bray, 1982). It is not clear whether the atypical axo-glial associations in the ROJ described here reflect the unique microenvironment of the ROJ affecting the development of conventional axo-glial associations.

Observations on the ROJ may be relevant to mechanisms underlying the maintenance of nodal membrane. It has been suggested that the axo-glial junctions on either side of the node function to restrict the lateral mobility of intercalated membrane proteins (Rosenbluth, 1976). Alternatively, the dense undercoating of nodal membrane may function to maintain the integrity of this specialized membrane (Ellisman, 1977; Waxman & Quick, 1978), or extracellular elements may play a role in anchoring specialized nodal proteins (Deerinck & Ellisman, 1984; Waxman & Ritchie, 1985). If paranodal terminal loops are a major factor in maintaining axolemma with nodal membrane character (i.e. high density of E-face IMPs and high percentage of large particles), then, assuming that there is lateral mobility of the particles within the plane of the membrane, the absence of one of the paranodal junctions (heminodal segment) might be expected to result in IMPs becoming homogeneously distributed over the membrane. In the transition zone of the ROJ, heminodal membrane does not exhibit typical nodal characteristics (present study; Hildebrand *et al.*, 1985). Descriptions of heminodal axolemma within dystrophic mice spinal roots are contradictory. Rosenbluth (1981a) reported that, while some degree of E-face particle aggregation may occur at these sites, typical annular concentrations of E-face IMPs were not observed. In contrast, Ellisman (1979) described heminodal E- and P-faces with IMP densities similar to those of typical nodal axolemma, with each fracture face having a distribution of particle sizes that was similar to that of respective faces

within normal nodes. In this regard, Waxman *et al.* (1978) described, on the basis of cytochemical studies, a spectrum of nodal membrane morphologies in these mutants. How these differing observations can be reconciled is not clear at this time, although they may represent a continuum of axolemmal ultrastructure at heminodal regions in dystrophic spinal roots.

At sites where oligodendroglial processes indent nodal membrane and establish a strip of paranodal-like axolemma, there is a focal reduction in the density of E-face particles. It is interesting, in this context, that in glial cell-deprived systems, E-face IMP densities of unsheathed axons (which would normally be myelinated) remain significantly higher than in internodal membrane of normal animals (Black *et al.*, 1985). These observations can be interpreted as suggesting that some modes of oligodendroglial ensheathment result in a suppression of membrane excitability. This suppression appears to be focal, and can even be limited to the area covered by a single aberrant oligodendrocytic process. Thus, while we (Waxman & Foster, 1980; Black *et al.*, 1985) and others (Wiley-Livingston & Ellisman, 1981; Oaklander *et al.*, 1984) believe that sodium-channel deployment does not depend on myelination, the localization of the channels appears to be modulated, as suggested by Rosenbluth (1983), by focal interactions with glial cells. Even in the context of the relatively chaotic axo-glial relations within the ROJ, some aspects of the interactions between axons and glial cells exhibit a high degree of specificity.

Acknowledgements

The authors wish to thank Mary E. Smith for excellent technical assistance. This work was supported in part by grants from the NINCDS (NS-15320), the National Multiple Sclerosis Society (RG-1231), the Medical Research Service, Veterans Administration, and the Swedish Medical Research Council (3761), Karolinska Institutet. During part of this work, JAB was supported by the Allen Charitable Trust, and CH was a visiting scientist at Stanford University, supported by the Folger Foundation.

References

AGUAYO, A. J. & BRAY, G. M. (1982) Developmental disorders of myelination in mouse mutants. In *Neuronal-glial Cell Interrelationships* (edited by SEARS, T. A.), pp. 57–76. Berlin, Heidelberg, New York: Springer-Verlag.

BLACK, J. A., FOSTER, R. E. & WAXMAN, S. G. (1981) Freeze-fracture ultrastructure of rat C.N.S. and P.N.S. nonmyelinated axolemma. *Journal of Neurocytology* **10**, 981–93.

BLACK, J. A., FOSTER, R. E. & WAXMAN, S. G. (1982a) Rat optic nerve: freeze-fracture studies during development of myelinated axons. *Brain Research* **250**, 1–20.

BLACK, J. A., FOSTER, R. E. & WAXMAN, S. G. (1983) Freeze-fracture ultrastructure of developing and adult non-myelinated ganglion cell axolemma in the retinal nerve fibre layer. *Journal of Neurocytology* **12**, 201–12.

BLACK, J. A., SIMS, T. J., WAXMAN, S. G. & GILMORE, S. A. (1985) Membrane ultrastructure of developing axons in glial cell deficient rat spinal cord. *Journal of Neurocytology* **14**, 78–104.

BLACK, J. A., WAXMAN, S. G. & FOSTER, R. E. (1982b) Spatial heterogeneity of the axolemma of non-myelinated fibers in the optic disc of the adult rat: freeze-fracture observations. *Cell and Tissue Research* **224**, 239–246.

BLACK, J. A., WAXMAN, S. G. & HILDEBRAND, C. (1984) Membrane specialization and axo-glial association in the rat retinal nerve fibre layer: freeze-fracture observations. *Journal of Neurocytology* **13**, 417–30.

BRAY, G. M., DUNCAN, I. D. & GRIFFITHS, I. R. (1983) 'Shaking pups': a disorder of central myelination in the spaniel dog. IV. Freeze-fracture electron microscopic studies of axons, oligodendrocytes and astrocytes in the spinal cord white matter. *Neuropathology and Applied Neurobiology* **9**, 355–368.

BRAY, G. M., RASMINSKY, M. & AGUAYO, A. J. (1981) Interactions between axons and their sheath cells. *Annual Review of Neuroscience* **4**, 127–62.

CONTI, F., HILLE, B., NEUMCKE, B., NONNER, W. & STÄMPLFI, R. (1976) Conductance of the sodium channels in myelinated nerve fibres with moderate sodium inactivation. *Journal of Physiology* **262**, 729–42.

DEERINCK, T. J. & ELLISMAN, M. H. (1984) Transcellular filaments at the node of Ranvier. *Neurosciences Abstracts* **10**, 163.

ELLISMAN, M. H. (1977) High voltage electron microscopy of cortical specializations associated with membranes at nodes of Ranvier. *Journal of Cell Biology* **75**, 108a.

ELLISMAN, M. H. (1979) Molecular specializations of the axon membrane at nodes of Ranvier are not dependent upon myelination. *Journal of Neurocytology* **8**, 719–35.

ELFVIN, L. G. (1961) The ultrastructure of the nodes of Ranvier in cat sympathetic fibers. *Journal of Ultrastructure Research* **5**, 374–87.

HILDEBRAND, C. (1971) Ultrastructural and light-microscopic studies of the developing feline spinal cord white matter. I. The nodes of Ranvier. *Acta physiologica scandinavica*, Suppl. **364**, 81–109.

HILDEBRAND, C., REMAHL, S. & WAXMAN, S. G. (1985) Axo-glial relations in the retina–optic nerve junction of the adult rat: electron-microscopic observations. *Journal of Neurocytology* **14**, 597–617.

HILDEBRAND, C. & WAXMAN, S. G. (1983) Regional node-like membrane specializations in non-myelinated axons of rat retinal nerve fiber layer. *Brain Research* **258**, 23–32.

HILDEBRAND, C. & WAXMAN, S. G. (1984) Postnatal differentiation of rat optic nerve fibers: electron microscopic observations on the development of nodes of Ranvier and axoglial relations. *Journal of Comparative Neurology* **224**, 25–37.

KRISTOL, C., AKERT, K., SANDRI, C., WYSS, U. R., BENNETT, M. V. L. & MOOR, H. (1977) The Ranvier nodes in the neurogenic electric organ of the knifefish *Sternarchus*: a freeze-etching study on the distribution of membrane-associated particles. *Brain Research* **125**, 197–212.

KRISTOL, C., SANDRI, C. & AKERT, K. (1978) Intramembranous particles at the nodes of Ranvier of the cat spinal cord: a morphometric study. *Brain Research* **142**, 391–400.

OAKLANDER, A. L., PELLEGRINO, R. G. & RITCHIE, J. M. (1984) Saxitoxin binding to central and peripheral nervous tissue of the myelin deficiency (md) mutant rat. *Brain Research* **307**, 393–7.

OLDFIELD, B. J. & BRAY, G. M. (1982) Differentiation of the nodal and internodal axolemma in the optic nerves of neonatal rats. *Journal of Neurocytology* **11**, 627–40.

PETERS, A. (1966) The node of Ranvier in the central nervous system. *Quarterly Journal of Experimental Physiology* **51**, 229–36.

QUICK, D. C., KENNEDY, W. R. & DONALDSON, L. (1979) Dimensions of myelinated nerve fibers near the motor and sensory terminals in cat tenuissimus muscle. *Neuroscience* **4**, 1089–96.

REVENKO, S. V., TIMIN, Y. N. & KHODOROV, B. I. (1973) Special features of the conduction of nerve impulses from the myelinated part of the axon into the non-myelinated terminal. *Biofizika* **18**, 1074–8.

RITCHIE, J. M. & ROGART, R. B. (1977) Density of sodium channels in mammalian myelinated nerve fibers and the nature of the axonal membrane under the myelin sheath. *Proceedings of the National Academy of Sciences, USA* **74**, 211–5.

ROSENBLUTH, J. (1976) Intramembranous particle distribution at the node of Ranvier and adjacent axolemma in myelinated axons of the frog brain. *Journal of Neurocytology* **5**, 731–45.

ROSENBLUTH, J. (1979) Aberrant axon–Schwann cell junctions in dystrophic mouse nerves. *Journal of Neurocytology* **8**, 655–72.

ROSENBLUTH, J. (1981a) Axoglial junctions in the mouse mutant Shiverer. *Brain Research* **208**, 283–97.

ROSENBLUTH, J. (1981b) Freeze-fracture approaches to ionophore localization in normal and myelin-deficient nerves. In *Demyelinating Disease: Basic and Clinical Electrophysiology* (edited by WAXMAN, S. G. & RITCHIE, J. M.), pp. 391–418. New York: Raven Press.

ROSENBLUTH, J. (1983) Structure of the node of Ranvier. In *Structure and Function in Excitable Cells* (edited by CHANG, D. C., TASAKI, I., ADELMAN, W. J. & LEUCHTAG, R.), pp. 25–52. New York: Plenum Press.

WAXMAN, S. G. (1977) Conduction in myelinated, unmyelinated, and demyelinated fibers. *Archives of Neurology* **34**, 585–9.

WAXMAN, S. G., BRADLEY, W. G. & HARTWIEG, E. A. (1978) Organization of the axolemma in amyelinated axons: a cytochemical study in dy/dy dystrophic mice. *Proceedings of the Royal Society of London, Series B* **201**, 301–8.

WAXMAN, S. G. & BRILL, M. H. (1978) Conduction through demyelinated plaques in multiple sclerosis: computer simulations of facilitation by short internodes. *Journal of Neurology, Neurosurgery and Psychiatry* **41**, 408–17.

WAXMAN, S. G. & FOSTER, R. E. (1980) Development of the axon membrane during differentiation of myelinated fibres in spinal nerve roots. *Proceedings of the Royal Society of London, Series B* **209**, 441–6.

WAXMAN, S. G. & QUICK, D. C. (1978) Intra-axonal ferric ion–ferrocyanide staining of nodes of Ranvier and initial segments in central myelinated fibers. *Brain Research* **144**, 1–10.

WAXMAN, S. G. & RITCHIE, J. M. (1985) Organization of ion channels in the myelinated nerve fiber. *Science* **228**, 1502–7.

WILEY-LIVINGSTON, C. A. & ELLISMAN, M. H. (1981) Development of axonal membrane specializations defines nodes of Ranvier and precedes Schwann cell myelin elaboration. *Developmental Biology* **79**, 344–55.